ACS central science

Research Article

http://pubs.acs.org/journal/acscii

A Compartmentalized Out-of-Equilibrium Enzymatic Reaction Network for Sustained Autonomous Movement

Marlies Nijemeisland,[†,‡] Loai K. E. A. Abdelmohsen,[†,‡] Wilhelm T. S. Huck,[*,†] Daniela A. Wilson,[*,†] and Jan C. M. van Hest[*,†,§]

[†]Institute for Molecules and Materials, Radboud University Nijmegen, Heyendaalseweg 135, 6525 AJ Nijmegen, The Netherlands

[§]Department of Biomedical Engineering and Chemical Engineering & Chemistry, Eindhoven University of Technology, PO Box 513, 5600 MB Eindhoven, The Netherlands

Supporting Information

ABSTRACT: Every living cell is a compartmentalized out-of-equilibrium system exquisitely able to convert chemical energy into function. In order to maintain homeostasis, the flux of metabolites is tightly controlled by regulatory enzymatic networks. A crucial prerequisite for the development of lifelike materials is the construction of synthetic systems with compartmentalized reaction networks that maintain out-of-equilibrium function. Here, we aim for autonomous movement as an example of the conversion of feedstock molecules into function. The flux of the conversion is regulated by a rationally designed enzymatic reaction network with multiple feedforward loops. By compartmentalizing the network into bowl-shaped nanocapsules the output of the network is harvested as kinetic energy. The entire system shows sustained and tunable microscopic motion resulting from the conversion of multiple external substrates. The successful compartmentalization of an out-of-equilibrium reaction network is a major first step in harnessing the design principles of life for construction of adaptive and internally regulated lifelike systems.

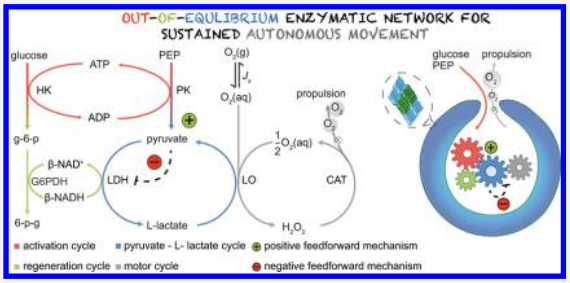

INTRODUCTION

The cellular environment can be regarded as a highly complex medium, in which numerous multistep enzymatic processes take place simultaneously with unsurpassed efficiency and specificity. One of the most striking characteristics of enzymatic reaction networks in living systems is their ability to generate a sustained output under out-of-equilibrium conditions as a result of built-in regulatory mechanisms. We identify an out-of-equilibrium state as a situation in which a continuous supply of energy is required to maintain a stationary state for extended periods of time. The system would end up in a thermodynamic minimum state when the energy supply stops. In nature, for example, feedback and feedforward motifs have evolved as mechanisms for maintaining homeostasis or dynamic equilibrium, and for fine-tuning metabolic flux.[1−3] Examples of regulatory mechanisms in metabolic networks include post-translational modifications which provide feedback mechanisms for metabolites[4] or small molecules that affect metabolic flux by allosteric effects on enzymes. It has also been suggested that the rapid amplification of responses against weak stimuli is partly due to the existence of feedforward activation via substrate cycles.[5,6] The general aim of these features in enzymatic networks is to regulate metabolite concentrations needed to match the local requirements.[7] The bottom-up construction of streamlined synthetic cells requires multicomponent enzymatic networks that carry out controllable user-defined functions that are regulated by external and internal factors.[7] However, these processes consume energy and inevitably decay toward equilibrium once their reactants are transformed into the desired products.

Therefore, much emphasis has been placed on the construction of multistep enzymatic cascades,[8,9] whereas the rational design of out-of-equilibrium enzymatic networks[10−12] has still proved very challenging. Crucially, the output of reaction cascades is simply the formation of a final product at a rate dependent on the slowest conversion step, and when the starting materials start to be consumed, the output slowly decays to zero. In contrast, reaction networks can produce oscillatory, adaptive, or homeostatic outputs, all depending on the network motifs. By implementing regulatory mechanisms, a system can be maintained at steady state for a prolonged time over a wider range of substrate concentrations than can be accomplished with a regular cascade process.

Previously we have reported the osmotic pressure induced shape transformation of poly(ethylene glycol)-*b*-poly(styrene) (PEG−PS) spherical polymersomes into bowl-shaped structures called stomatocytes.[13−15] These stomatocytes were turned into nanomotors by simply encapsulating active nanoparticles (e.g., platinum) and enzymes (e.g., catalase) in the nanocavity.[14,15] Substrate (fuel) conversion by the confined catalysts in the small compartment led to propulsion of the stomatocytes, of which the speed was dependent on the fuel concentration. Herein, we report on a non-natural regulatory

Received: August 31, 2016
Published: November 9, 2016

DOI: 10.1021/acscentsci.6b00254
ACS Cent. Sci. 2016, 2, 843−849

metabolic network compartmentalized in a stomatocyte which shows tunable and sustained performance under out-of-equilibrium conditions. The confined network allows the conversion of multiple natural substrates (Figure 1A) via four

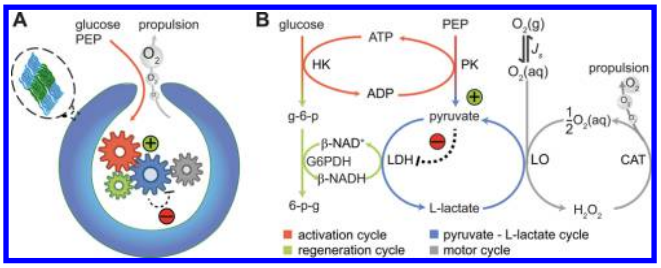

Figure 1. Rational design and experimental assembly of a compartmentalized metabolic network. (A) Schematic representation of the nanoreactors containing four enzymatic cycles which are able to convert glucose and phosphoenolpyruvate (PEP) into movement of the construct. (B) Rational design of a metabolic pathway for double cycling of natural substrates leading to autonomous movement. The activation cycle, starting with glucose and phosphoenolpyruvate, feeds forward the pyruvate−L-lactate cycle with regeneration of β-NADH, and is controlled by the amount of ATP present in the system. The negative feedforward regulation by pyruvate enables a tunable continuous local production of oxygen by the motor cycle. Sufficient concentrations of glucose and PEP as well as positive and negative feedforward mechanisms are crucial for maintaining a prolonged out-of-equilibrium state.

metabolic modules into hydrogen peroxide, which is converted into molecular oxygen in the final step. Encapsulation of the enzymatic network in bowl-shaped polymeric nanoparticles represents an example of a compartmentalized out-of-equilibrium system that is capable of converting molecular fuels into motion.[16−22] Regulating the turnover rates in the enzymatic network leads to a tunable and sustained output and a concomitant control over the speed of the nanomotors.

The construct is in effect able to adapt its behavior to the changes in the concentration of natural substrates by regulating their consumption to produce sustained movement with constant speed.

RESULTS AND DISCUSSION

Rational Design of a Tunable Metabolic Network. Inspired by the "functional units" or "modules" in evolved biochemical networks in cells,[23,24] a minimal biochemical reaction model was constructed to include features that can lead to tunable and sustainable energy production. The basic metabolic network was setup by an ATP-dependent activation module based on hexokinase (HK) and pyruvate kinase (PK) with a phosphate donor (phosphoenolpyruvate) and glucose as energy source (Figure 1B, activation cycle). It permits activation of the enzymatic network even when ATP levels are below physiological concentrations (<1 mM).[25,26] A feedforward activation was introduced in which the output of the activation cycle, pyruvate, acts as a trigger molecule for the pyruvate−L-lactate cycle. In this cycle, L-lactate dehydrogenase (LDH) consumes pyruvate and this reaction is opposed by L-lactate oxidase (LO) catalyzing the reaction in the opposite direction. By continuous injection of pyruvate, the cycle speeds up until a steady state is reached due to feedforward inhibition at high concentrations of pyruvate on LDH (Figure 1B, pyruvate−L-lactate cycle).[27] A concurrent flux through this cycle occurs when an excess of β-NADH is present, which is continuously regenerated by the conversion of glucose-6-phosphate by glucose-6-phosphate dehydrogenase (G6PDH) into 6-phosphogluconolactone (6-p-g). This results in net hydrogen peroxide production. Since ATP determines the concentration of β-NADH, the concentration of ATP activates, but at the same time regulates the entire metabolic network. While in natural systems substrate cycles have sometimes been called futile cycles when there is no overall effect other than to dissipate heat,[28] in our network the function of the pyruvate−L-lactate cycle is coupled to our motor cycle containing catalase (CAT) (Figure 1B, motor cycle). Similar isolated motor cycles have been implemented before in nano- and micromotor systems (e.g., glucose oxidase/CAT), and the current understanding of their mechanism of motion is based on a combination of phoretic and bubble propulsion.[15,18,19,29,30] Herein the entire metabolic network is encapsulated in our polymeric capsule equipped with a nanopore; it is expected that the highly localized decomposition of hydrogen peroxide into oxygen leads to microscopic motion of the construct due to the combined action of fast escape of the oxygen through the opening and the accompanying local density fluctuations, giving rise to phoretic motion.

Evaluation of the Metabolic Network. We first simulated the enzymatic network using a mathematical model based on a set of ordinary differential equations (ODEs). Kinetic parameters were measured experimentally from single-enzyme experiments or obtained from literature and used as input for the simulations (see Table S1 and Figure 2A,B). In all cases, dissolved oxygen consumption by LO is assumed to be not rate-limiting in the open reactor due to continuous replenishment from air. The oxygen concentration is therefore kept constant in the mathematical model. The response of the network to varying substrate concentrations was tested to provide us with a better insight into the key parameters that govern the steady state behavior of the network. The simulations show that ATP acts as an internal regulator of the network for the production of the O_2 precursor H_2O_2 (Figure 2C). The ATP concentration has an effect on the speed of activation (Figure 2C, inset), the cycling rate of the pyruvate−L-lactate cycle, and thus the rate of H_2O_2 production, when the system is saturated in glucose (2.5 mM) and PEP (10.0 mM). Therefore, the more ATP is present, the faster the reaction velocity of the pyruvate−L-lactate cycle increases, as the activation cycle is continuously injecting substrate into it (see Figure S1). In the initial phase, even a small quantity of ATP can speed up the rates of β-NAD^+/β-NADH cycling and H_2O_2 production, and thus the system acts as a chemical amplifier. This feedforward activation takes place when the concentrations of the cycling substrates are much lower than their respective Michaelis−Menten constants. Above these values, a negative substrate inhibition is observed (see Figure 2B). In the enzymatic network, this mechanism regulates the consumption of energy and slows down glucose consumption, which leads to a steady state phase. This elongates the out-of-equilibrium state and extends the *in situ* production of hydrogen peroxide (Figure 2D). In the activation cycle, hexokinase has a low K_m for glucose, so it permits activation of the enzymatic network even when glucose levels are below 1 mM.[31] Consequently, glucose only affects the duration of the steady state and does not affect the rate of hydrogen peroxide production. Importantly, as shown in Figure 2C,D, the H_2O_2 production is constant over extended (up to 3 h) time periods.

DOI: 10.1021/acscentsci.6b00254
ACS Cent. Sci. 2016, 2, 843−849

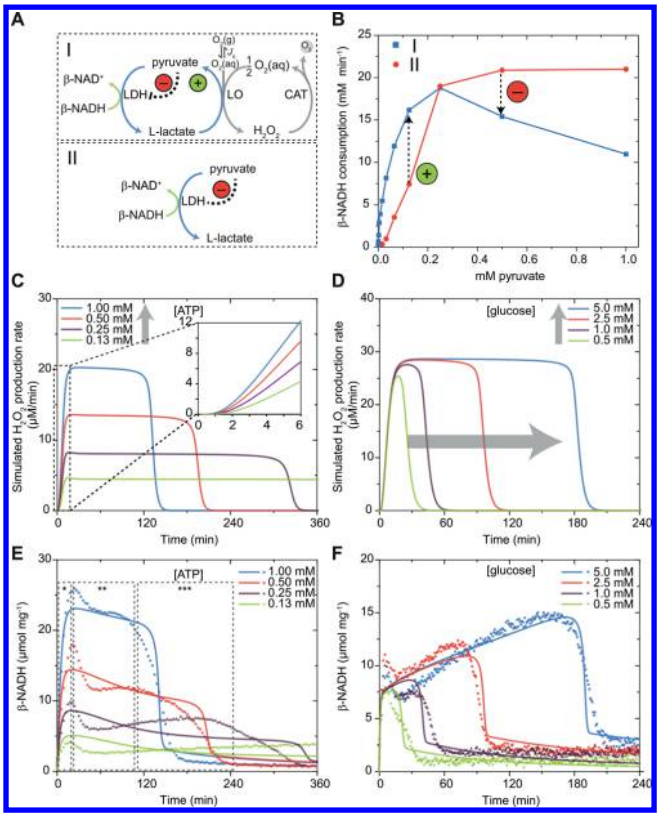

Figure 2. Characterization of the metabolic pathway. (A) Reaction scheme of the proposed assay for the pyruvate−L-lactate cycle and for the comparison with LDH activity. (B) β-NADH consumption rates of the pyruvate−L-lactate cycle and for LDH at varied concentrations of pyruvate. Below 0.5 mM a positive effect on the consumption rate is observed due to pyruvate regeneration. Negative substrate inhibition is observed for values higher than 0.5 mM pyruvate. (C, D) Time courses in H_2O_2 production rates for various values of initial [ATP] (C) and [glucose] (D) from model predictions. The inset shows an expansion of the graph near the coordinate origin. (E) Progress curves of β-NADH production and consumption per mg of enzyme mixture, obtained experimentally for different initial concentrations of ATP (0.13−1.0 mM) at fixed glucose concentrations (2.5 mM). Three regimes (*, **, and ***) are defined and represent different phases of operation of the enzymatic network. Solid lines represent model predictions using optimized parameters. (F) Progress curves of β-NADH production and consumption obtained experimentally for different initial concentrations of glucose (0.5−5.0 mM), while ATP concentrations were kept fixed at 0.5 mM. Solid lines represent model predictions using optimized parameters.

After simulating the general properties of the network, we experimentally determined the behavior of the enzymatic network in buffer solution, hereafter called bulk conditions, by monitoring β-NADH fluorescence in time. Figure 2E shows the data points of progress curves of β-NADH production and consumption during operation of the entire metabolic pathway at various concentrations of ATP. The initial increase in [β-NADH] (see regime * in Figure 2E) can be explained by the ATP-dependent formation of glucose-6-phosphate, which fuels the regeneration process of β-NADH out of β-NAD^+; the higher the initial [ATP], the stronger the initial increase in [β-NADH]. Subsequently, the pyruvate−L-lactate cycle becomes fueled with pyruvate (see regime **, Figure 2E), which starts to consume β-NADH rapidly, but seems to converge into a steady state with nearly similar rates of β-NADH production and consumption. After several hours, when glucose becomes depleted, a fast decrease in [β-NADH] is measured and the enzymatic network stops working (regime ***, Figure 2E). Again, this decrease is more pronounced with increased starting levels of ATP. This indicates that the pyruvate−L-lactate cycle is accelerated when more ATP is present. The same trend is observed for varied glucose concentrations, however glucose affects only the length of the steady state (Figure 2F). Our mathematical model is fitted to the experimental data of both glucose and ATP concentration versus time, by minimizing the difference between model simulations and the experimental data. The simulated data (solid lines) are qualitatively good fits to the experimental data, providing confirmation that our model represents the key reactions in the network and that classical enzyme kinetics can be used to predict and optimize the behavior of the enzymatic network.

Compartmentalization of the Metabolic Network. After establishing the conditions under which the enzymatic network leads to sustained hydrogen peroxide production, the entire pathway was encapsulated in stomatocytes via the controlled shape transformation of polymersomes made from poly(ethylene glycol)$_{44}$-*b*-poly(styrene)$_{167}$ amphiphilic block copolymers following previously reported preparation conditions from our group.[15] The preparation entailed a two-step process. First, spherical polymersomes were transformed in open-neck stomatocytes in a medium of water and organic solvent. After dialysis, to remove excess organic solvent, the open-neck stomatocytes were plasticized with a small amount of organic solvent to induce the formation of closed-neck stomatocytes in the presence of the enzymatic network, with a total protein concentration of 17.2 mg mL^{-1}. Small to almost closed neck stomatocytes (<5 nm) were mostly obtained.[15] The bowl-shaped structures were confirmed with cryo-transmission electron microscopy, transmission electron microscopy, and energy dispersive X-ray spectroscopy, see Figure 3A and Figure S2. The encapsulation of the enzymatic network was evaluated with SDS−PAGE densitometry. For this experiment, the enzymes were released from the nanoreactors by reshaping the bowl-shaped structures back into polymersomes by the addition of organic solvent (Figure S3). A recovery of enzymes from the nanoreactors up to 22% was found from an initial feed concentration of 17.2 mg mL^{-1} (total enzyme concentration before closure of the nanoreactor), see Supporting Information section 2.3. As was found previously, this is significantly higher than statistical encapsulation and is possibly due to a templating effect.[8,15] The protein profiles for the released enzymes were furthermore comparable with bulk enzyme solutions and indicate a similar enzyme composition inside the nanoreactors (Figure 3B).

The nanoreactor activity was tested by following β-NADH fluorescence over time upon substrate addition. As observed in our bulk experiments, the β-NADH levels initially increase due to the production of glucose-6-phosphate from glucose by the activation cycle (Figure 3C) and then reach a steady state. Initial slopes obtained from the nanoreactor assays were compared with slopes from a standard concentration row of the enzyme mix in bulk. Based on activity, a loading efficiency of 32 ± 4% was found (see Supporting Information section 2.3). These results confirm that the enzymes have retained their activity. Gratifyingly, we were able to fit experimental data from the bulk system and compartmentalized networks using the same mathematical model, providing further evidence that the main properties of the network are not altered during compartmentalization.

DOI: 10.1021/acscentsci.6b00254
ACS Cent. Sci. 2016, 2, 843−849

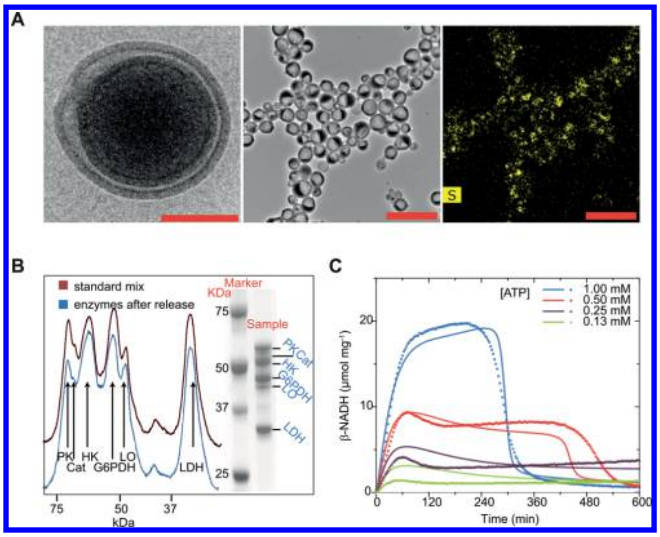

Figure 3. Characterization of the nanoreactors. (A) Cryo-transmission electron microscopy (cryo-TEM) image of a nanoreactor (left). TEM image of nanoreactors loaded with the enzymatic network (middle). TEM coupled with energy dispersive X-ray spectroscopy showing the mapping of sulfur (S), specific to the cysteines and methionines in the enzymes and their localization inside the nanoreactors (right). Scale bars 100 nm (left) and 1 μm (middle and right). (B) Intensity profile of an SDS−PAGE lane, loaded with enzymes recovered from reopened nanoreactors (left). SDS−PAGE shows the bands from the enzymes of the network (right). (C) Time courses for the encapsulated enzymatic network, depicting β-NADH production and consumption for various initial concentrations of ATP.

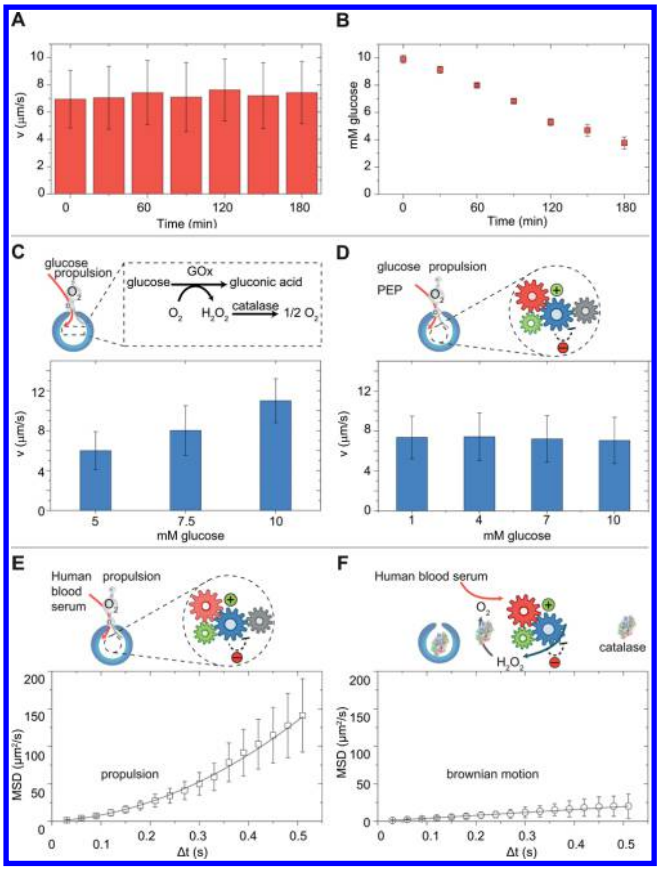

Figure 4. Nanoreactors movement analysis. (A) Average speeds of the nanoreactors over time, with 10 mM glucose as starting concentration. For every time point, average speeds were calculated from the MSDs of 60 particles over 90 s. (B) Experimentally determined glucose concentrations over time. The depletion of glucose does not influence the nanoreactor speed (A). (C) Average initial speeds (first 90 s) of nanoreactors loaded with an enzymatic cascade and fueled with different glucose concentrations. (D) Average speeds (first 90 s) of nanoreactors containing enzymatic network at different glucose concentrations. (E) Nanoreactor movement in human serum with the full network compartmentalized. (F) Motion of nanoreactors loaded with catalase only; the remainder of the network is added to the serum.

Analysis of Movement of the Nanoreactors. After demonstrating that the enzymatic pathway can be entrapped efficiently in the cavity of the assembly, the sustained autonomous movement driven by the enzymatic network was investigated. The conversion of chemical energy into movement was analyzed with nanoparticle-tracking analysis (NTA). This technique uses laser light scattering combined with a charge-coupled device camera to track the movement of the particles in real time (Figure S4).

Nanoreactors loaded with the enzymatic network, substrates, and cofactors were mixed with empty nanoreactors (1:9 v/v) and were measured with NTA. Autonomous movement of the nanoreactors in the presence of substrates (10 mM glucose) and cofactors was observed (see Movie S1). Directional propulsive motion which is in common agreement with our previous studies using stomatocyte nanomotors was observed.[14,15,32] Over a period of 3 h, individual trajectories were measured by NTA in order to derive average mean square displacements (MSD). At every time point, 60 particles were tracked for 90 s and average speeds were calculated over this time period (Figure 4A). At the same time point, the glucose concentration was determined experimentally (Figure 4B). Figure 4A shows steady movement speed during glucose consumption. Control experiments were performed by the addition of fuel to empty nanoreactors (see Movie S2) or filled nanoreactors without fuel (see Movie S3). No change in their Brownian motion was observed.

These results demonstrate the crucial importance of enzymatic networks to drive displacement: independently of the glucose concentrations, and during considerable reaction times, the output of the network (H_2O_2 production rate) is more or less constant for hours.

To further demonstrate the out-of-equilibrium behavior of the encapsulated enzymatic network, a control experiment was performed with nanoreactors loaded with a well-studied 2-step enzymatic cascade based on glucose oxidase (GOx) and catalase, which directly runs to an equilibrium.[15] For a valid comparison of the two systems, it was chosen to fuel stomatocytes with the enzymatic network and stomatocytes with the 2-step enzymatic cascade with various concentrations of glucose. The relatively very slow glucose conversion by GOx from the enzymatic cascade made it experimentally difficult to obtain reliable speed data due to sedimentation in the measuring chamber. The starting concentration of glucose was therefore varied, and average speeds were measured over 90 s directly after addition of glucose. The compartmentalized 2-step enzymatic cascade produces the same output in terms of reaction product but clearly not in terms of movement characteristics regarding prolonged duration and maintaining speeds. Using the GOx/CAT system, a direct correlation between the velocity of the nanoreactors and glucose levels was observed (Figure 4C), opposed to the network in the similar

DOI: 10.1021/acscentsci.6b00254
ACS Cent. Sci. 2016, 2, 843−849

fuel regime.[33] Nanoreactors with the enzymatic network exhibit relatively constant speeds at various glucose concentrations until glucose is depleted (Figure 4D). These results qualitatively show the difference between using this network and enzyme cascades for operating such nanomotors using glucose as fuel.[15] It should be noted that the rates of glucose conversion will be affected by the use of different metabolic enzymes in the network and the cascade (GOx and HK) with a much lower K_m value for HK for glucose (K_m = 0.02 mM) than GOx (K_m = 33−110 mM); the comparative study with different glucose levels however still clearly indicates the fundamentally distinct behavior of enzymatic cascade and network systems.

In effect this experiment emphasizes the ability of the compartmentalized out-of-equilibrium enzymatic network by regulating the fuel consumption and maintaining constant speeds of the particles. In contrast, this is not possible in a simple 2-step enzymatic cascade system.

To confirm the regulatory function of ATP on the performance of the nanoreactor, the concentration of ATP was varied from 0.25 mM to 1 mM and an approximately 40% increase in propulsion speed was observed over this regime (Figure S5). This increase can also be rationalized by our mathematical model, which shows an increase in hydrogen peroxide production rates when ATP concentrations are increased. This is in agreement with the stable average speeds we observed experimentally. The design of the network and the obtained steady state allow for a constant speed of the particles even at variable fuel concentrations by regulating its fuel consumption.

We note that the enzymatic network *consumes* oxygen, as for every mole of oxygen consumption by LO, the catalase produces 1/2 mol of oxygen for every mole of glucose oxidized. However, the system *produces* oxygen locally (as observed by visible bubble formation after prolonged reaction times at high glucose concentrations), and the oxygen consumed in the beginning of the final cycle is replenished by the time hydrogen peroxide is converted into oxygen. To demonstrate this hypothesis, first, in a closed system, oxygen depletion was measured over a 2 h period (see Figure S6). In an open system, however, the oxygen level in solution remained constant, indicating that the mass transfer rate of O_2 over the air−liquid interface is greater than the net O_2 consumption by the enzymatic network. Besides particle motion through local O_2 production, we hypothesize that the final reaction in our network, the decomposition of H_2O_2 into O_2 and H_2O, can locally (in the lumen of these nanoreactors) create density fluctuations which contribute to the particle propulsion via diffusiophoresis as well.[34,35] The movement of the nanomotors and the behavior of the resulting MSD curves (e.g., Figure 4E) are in agreement with a self-diffusiophoretic model,[35−38] showing clearly nonlinear fitting according to the equation $\langle r^2 \rangle = 4D\Delta t + (v\Delta t)^2$, and from which the velocity of our stomatocytes particles was extracted.

Finally, the protective element of compartmentalization and the effect of confinement were evaluated by performing an experiment in a complex chemical medium, such as human blood serum (HBS). HBS was chosen as it contains many different proteins and enzymes, including catalase. Nanoreactors were mixed with human blood serum, and their movement was measured by means of NTA (Figure 4E). The glucose (4 mM) and L-lactate (0.08 mM) levels in the serum were more than sufficient to induce movement of the nanoreactors. A similar experiment was performed with nanoreactors loaded with only catalase (Figure 4F). The enzymes that together produce H_2O_2 were added to human blood serum. H_2O_2 was thus produced not in the cavity but in bulk, whereas catalase inside the nanoreactors could employ this fuel to induce movement. No movement was observed, however, most probably as a result of the fact that H_2O_2 concentration was lowered to such an extent that the entrapped catalase cannot induce propulsion anymore. Enzyme compartmentalization therefore allows for *in situ* local O_2 production that directly acts as driving force for efficient movement.

CONCLUSIONS

In summary, we have designed and constructed a compartmentalized network which is able to show a regulated, sustained performance under out-of-equilibrium conditions; it allows the conversion of chemical energy into motion by using natural components in a protected environment. Contrary to a simple 2-step enzymatic cascade, the out-of-equilibrium enzymatic network is able to regulate the fuel consumption while maintaining constant speeds of the particles. In the context of bottom-up synthetic biology, we anticipate that this out-of-equilibrium metabolic network concept can be extended to other functions than motion, thereby providing a significant advance in the development of molecular lifelike systems.

METHODS

All chemicals and enzymes were used as received unless otherwise stated. β-NADH, β-NAD^+, ATP magnesium salt, D-glucose (glucose), glucose-6-phosphate (g-6-p), sodium phosphoenolpyruvate (PEP), sodium pyruvate, sodium L-lactate, magnesium chloride, human blood serum (HBS, from male AB clotted whole blood, sterile filtered, USA origin), pyruvate kinase from rabbit muscle (PK, EC 2.7.1.40, 475 units mg^{-1}), L-lactate dehydrogenase recombinant from *Escherichia coli* (LDH, EC 1.1.1.27, 257 units mg^{-1}), catalase from bovine liver (CAT, 3750 units mg^{-1}, EC 1.11.1.6), glucose oxidase from *Aspergillus niger* type II, (GOx, E.C. 1.1.3.4) lyophilized powder 228.25 U mg^{-1}, anisole, *N*,*N*,*N*′,*N*″,*N*″-pentamethyldiethylenetriamine (PMDETA), copper(I) bromide, dichloromethane, styrene, magnesium sulfate, horseradish peroxidase (HRP), 10-acetyl-3,7-dihydroxyphenoxazine (Ampliflu Red), and methanol were obtained from Sigma-Aldrich. L-Lactate oxidase from *Pediococcus* species (LO, EC 1.1.3.2, 1000 units mg^{-1}) was received from BBI Enzymes. Hexokinase from *Saccharomyces cerevisiae* (HK, EC 2.7.1.1, 202 units mg^{-1}) and glucose-6-phosphate dehydrogenase from *Leuconostoc mesenteroides* (G6PDH, EC 1.1.1.363, 507 units mg^{-1}) were purchased from Worthington. Stock solutions of all enzymes (10 mg mL^{-1}) and substrates were prepared in 100 mM KPi (pH 7.0) containing 10 mM magnesium chloride. For the block copolymer synthesis, styrene was distilled to remove the inhibitor. Ultrapure Milli-Q water was obtained with a Labconco Water Pro PS purification system (18.2 MΩ) and was used for the procedures of polymersome self-assembly and their dialysis. Dialysis membranes MWCO 12000−14000 g/mol Spectra/Por were used for dialysis. Ultrafree-MC centrifugal filters 0.22 μm were purchased from Millipore. Sodium nitrate was purchased from Merck. 4× Laemmli Sample Buffer and the protein marker (Precision Plus Protein Prestained Dual Color) were purchased from Bio-Rad.

Poly(ethylene glycol)$_{44}$-*b*-poly(styrene)$_{167}$ Synthesis. Synthesis of this polymer was performed using atom transfer

DOI: 10.1021/acscentsci.6b00254
ACS Cent. Sci. 2016, 2, 843−849

radical polymerization (ATRP), as previously reported in the literature.[13] ^{1}H NMR and GPC were used to determine the length and the polydispersity. Detailed synthetic procedures are described in Supporting Information section 2.3.

Kinetic Analysis of Enzymatic Network (Bulk). A reaction mixture was prepared containing final concentrations of 10 mM PEP, 500 μM β-NAD$^+$, pyruvate kinase (PK, 0.5 unit mL^{-1}), HK (0.3 unit mL^{-1}), G6PDH (0.6 unit mL^{-1}), L-lactate dehydrogenase (LDH, 0.1 unit mL^{-1}), L-lactate oxidase (LO, 0.2 unit mL^{-1}), and catalase (CAT, 2.2 units mL^{-1}). For evaluating the effect of ATP, varying concentrations of a stock solution of 80 mM ATP were added. The reaction was started by the addition of glucose with a final concentration of 2.5 mM in a total reaction volume of 300 μL. The effect of glucose was tested by adding different concentrations of an 80 mM glucose stock solution. By the addition of ATP to a final concentration of 500 μM in a 300 μL reaction volume, the reaction was started. Progress of the reaction was monitored directly by measuring β-NADH fluorescence.

Kinetic Analysis of Nanoreactors. Nanoreactors containing the enzymatic network were diluted with buffer, containing 500 μM β-NAD$^+$ and 10 mM PEP, to obtain a final dilution factor of 900. For evaluating the effect of ATP, varying concentrations of a stock solution of 80 mM ATP were added. The reaction was started by the addition of glucose with a final concentration of 2.5 mM in a total reaction volume of 300 μL. The effect of glucose was tested by adding different concentrations of an 80 mM glucose stock solution. By the addition of ATP to a final concentration of 500 μM in a 300 μL reaction volume, the reaction was started. Progress of the reaction was monitored directly by measuring β-NADH fluorescence.

Sustained Autonomous Movement of the Nanoreactors. The number of particles of stomatocytes encapsulating the network was adjusted to values between 10^7 and 10^9 using buffer that contains PEP and all cofactors; thereafter fuel was added (different concentrations of glucose), and the samples were injected into the Nanosight sample chamber. In order to tune the speed of the network encapsulating nanoreactors, glucose concentration was fixed while ATP concentration was varied.

■ ASSOCIATED CONTENT

Supporting Information

The Supporting Information is available free of charge on the ACS Publications website at DOI: 10.1021/acscentsci.6b00254.

Additional information regarding the mathematical modeling of the network, kinetic analysis of the network in bulk and nanoreactors, enzyme quantification, and moving analysis of the nanomotors (PDF)

Autonomous movement and Brownian motion of two populations of nanoreactors (MPG)

Brownian motion of empty nanoreactors with fuel (MPG)

Brownian motion of enzyme-containing nanoreactors without fuel (MPG)

■ AUTHOR INFORMATION

Corresponding Authors

*E-mail: w.huck@science.ru.nl.

*E-mail: d.wilson@science.ru.nl.

*E-mail: j.vanhest@science.ru.nl, J.C.M.v.Hest@tue.nl.

Author Contributions

‡M.N. and L.K.E.A.A. contributed equally to this work

Notes

The authors declare no competing financial interest.

■ ACKNOWLEDGMENTS

This work was supported by the European Research Council under the European Union's Seventh Framework Programme (FP7/2007-20012)/ERC-StG 307679 "StomaMotors". We acknowledge support from the Ministry of Education, Culture and Science (Gravitation program 024.001.035) and funding from Radboud University (Bionic Cell project). We would like to thank Geert-Jan Janssen from General Instruments, Radboud University for assistance with the Cryo-TEM analysis and TEM-EDX experiments. The authors thank David Foschepoth for valuable comments and suggestions.

■ ABBREVIATIONS

ATRP, atom transfer radical polymerization; PDI, polydispersity index; HK, hexokinase; PK, pyruvate kinase; G6PDH, glucose-6-phosphate dehydrogenase; LDH, L-lactate dehydrogenase; LO, L-lactate oxidase; Cat, catalase; GOx, glucose oxidase; MSD, mean square displacement; EDX, energy dispersive X-ray

■ REFERENCES

(1) Bernhard, S. A. The intracellular equilibrium thermodynamic and steady-state concentrations of metabolites. *Cell Biophys.* **1988**, *12*, 119−132.

(2) Tyson, J. J.; Chen, K.; Novak, B. Network dynamics and cell physiology. *Nat. Rev. Mol. Cell Biol.* **2001**, *2*, 908−916.

(3) Brandman, O.; Ferrett, J. E.; Li, R.; Meyer, T. Interlinked fast and slow positive feedback loops drive reliable cell decisions. *Science* **2005**, *310*, 496−498.

(4) Zhao, S.; Xu, W.; Jiang, W.; Yu, W.; Lin, Y.; Zhang, T.; Yao, J.; Zhou, L.; Zeng, Y.; Li, H.; Li, Y.; Shi, J.; An, W.; Hancock, S. M.; He, F.; Qin, L.; Chin, J.; Yang, P.; Chen, X.; Lei, Q.; Xiong, Y.; Guan, K.-L. Regulation of Cellular Metabolism by Protein Lysine Acetylation. *Science* **2010**, *327*, 1000−1004.

(5) Newsholme, E. A. Substrate cycles: their metabolic, energetic and thermic consequences in man. *Biochem. Soc. Symp.* **1978**, *43*, 183−205.

(6) Goldbeter, A.; Koshland, D. E. Ultrasensitivity in Biochemical Systems Controlled by Covalent Modification - Interplay between Zero-Order and Multistep Effects. *J. Biol. Chem.* **1984**, *259*, 14441−14447.

(7) Milo, R.; Shen-Orr, S.; Itzkovitz, S.; Kashtan, N.; Chklovskii, D.; Alon, U. Network motifs: Simple building blocks of complex networks. *Science* **2002**, *298*, 824−827.

(8) Peters, R. J. R. W.; Marguet, M.; Marais, S.; Fraaije, M. W.; van Hest, J. C. M.; Lecommandoux, S. Cascade Reactions in Multicompartmentalized Polymersomes. *Angew. Chem., Int. Ed.* **2014**, *53*, 146−150.

(9) Wendell, D.; Todd, J.; Montemagno, C. Artificial Photosynthesis in Ranaspumin-2 Based Foam. *Nano Lett.* **2010**, *10*, 3231−3236.

(10) Semenov, S. N.; Wong, A. S. Y.; van der Made, R. M.; Postma, S. G. J.; Groen, J.; van Roekel, H. W. H.; de Greef, T. F. A.; Huck, W. T. S. Rational design of functional and tunable oscillating enzymatic networks. *Nat. Chem.* **2015**, *7*, 160−165.

(11) He, X.; Aizenberg, M.; Kuksenok, O.; Zarzar, L. D.; Shastri, A.; Balazs, A. C.; Aizenberg, J. Synthetic homeostatic materials with chemo-mechano-chemical self-regulation. *Nature* **2012**, *487*, 214−218.

(12) Boekhoven, J.; Hendriksen, W. E.; Koper, G. J. M.; Eelkema, R.; van Esch, J. H. Transient assembly of active materials fueled by a chemical reaction. *Science* **2015**, *349*, 1075−1079.

(13) Kim, K. T.; Zhu, J. H.; Meeuwissen, S. A.; Cornelissen, J. J. L. M.; Pochan, D. J.; Nolte, R. J. M.; van Hest, J. C. M. Polymersome

DOI: 10.1021/acscentsci.6b00254
ACS Cent. Sci. 2016, 2, 843−849

Stomatocytes: Controlled Shape Transformation in Polymer Vesicles. *J. Am. Chem. Soc.* **2010**, *132*, 12522−12524.
(14) Wilson, D. A.; Nolte, R. J. M.; van Hest, J. C. M. Autonomous movement of platinum-loaded stomatocytes. *Nat. Chem.* **2012**, *4*, 268−274.
(15) Abdelmohsen, L. K. E. A.; Nijemeisland, M.; Pawar, G. M.; Janssen, G.-J. A.; Nolte, R. J. M.; van Hest, J. C. M.; Wilson, D. A. Dynamic Loading and Unloading of Proteins in Polymeric Stomatocytes: Formation of an Enzyme-Loaded Supramolecular Nanomotor. *ACS Nano* **2016**, *10*, 2652−2660.
(16) Ma, X.; Wang, X.; Hahn, K.; Sánchez, S. Motion Control of Urea-Powered Biocompatible Hollow Microcapsules. *ACS Nano* **2016**, *10*, 3597−3605.
(17) Bunea, A. I.; Pavel, I. A.; David, S.; Gaspar, S. Sensing based on the motion of enzyme-modified nanorods. *Biosens. Bioelectron.* **2015**, *67*, 42−48.
(18) Pantarotto, D.; Browne, W. R.; Feringa, B. L. Autonomous propulsion of carbon nanotubes powered by a multienzyme ensemble. *Chem. Commun.* **2008**, 1533−1535.
(19) Ma, X.; Jannasch, A.; Albrecht, U. R.; Hahn, K.; Miguel-Lopez, A.; Schaffer, E.; Sanchez, S. Enzyme-Powered Hollow Mesoporous Janus Nanomotors. *Nano Lett.* **2015**, *15*, 7043−7050.
(20) Schattling, P.; Thingholm, B.; Städler, B. Enhanced Diffusion of Glucose-Fueled Janus Particles. *Chem. Mater.* **2015**, *27*, 7412−7418.
(21) Kuchler, A.; Yoshimoto, M.; Luginbuhl, S.; Mavelli, F.; Walde, P. Enzymatic reactions in confined environments. *Nat. Nanotechnol.* **2016**, *11*, 409−420.
(22) Marguet, M.; Bonduelle, C.; Lecommandoux, S. Multicompartmentalized polymeric systems: towards biomimetic cellular structure and function. *Chem. Soc. Rev.* **2013**, *42*, 512−529.
(23) Lauffenburger, D. A. Cell signaling pathways as control modules: Complexity for simplicity? *Proc. Natl. Acad. Sci. U. S. A.* **2000**, *97*, 5031−5033.
(24) Han, J.-D. J.; Bertin, N.; Hao, T.; Goldberg, D. S.; Berriz, G. F.; Zhang, L. V.; Dupuy, D.; Walhout, A. J. M.; Cusick, M. E.; Roth, F. P.; Vidal, M. Evidence for dynamically organized modularity in the yeast protein-protein interaction network. *Nature* **2004**, *430*, 88−93.
(25) Gribble, F. M.; Loussouarn, G.; Tucker, S. J.; Zhao, C.; Nichols, C. G.; Ashcroft, F. M. A Novel Method for Measurement of Submembrane ATP Concentration. *J. Biol. Chem.* **2000**, *275*, 30046−30049.
(26) Larcombe-McDouall, J.; Buttell, N.; Harrison, N.; Wray, S. In vivo pH and metabolite changes during a single contraction in rat uterine smooth muscle. *J. Physiol.* **1999**, *518*, 783−790.
(27) Stambaugh, R.; Post, D. Substrate and Product Inhibition of Rabbit Muscle Lactic Dehydrogenase Heart (H4) and Muscle (M4) Isozymes. *J. Biol. Chem.* **1966**, *241*, 1462−1467.
(28) Reidy, S. P.; Weber, J.-M. Accelerated substrate cycling: a new energy-wasting role for leptin in vivo. *Am. J. Physiol.* **2002**, *282* (2), E312−E317.
(29) Ma, X.; Sanchez, S. A bio-catalytically driven Janus mesoporous silica cluster motor with magnetic guidance. *Chem. Commun.* **2015**, *51*, 5467−5470.
(30) Wu, Y. J.; Lin, X. K.; Wu, Z. G.; Mohwald, H.; He, Q. Self-Propelled Polymer Multilayer Janus Capsules for Effective Drug Delivery and Light-Triggered Release. *ACS Appl. Mater. Interfaces* **2014**, *6*, 10476−10481.
(31) Mulukutla, B. C.; Khan, S.; Lange, A.; Hu, W. S. Glucose metabolism in mammalian cell culture: new insights for tweaking vintage pathways. *Trends Biotechnol.* **2010**, *28*, 476−484.
(32) Peng, F.; Tu, Y. F.; van Hest, J. C. M.; Wilson, D. A. Self-Guided Supramolecular Cargo-Loaded Nanomotors with Chemotactic Behavior towards Cells. *Angew. Chem., Int. Ed.* **2015**, *54*, 11662−11665.
(33) Gibson, Q. H.; Swoboda, B. E.; Massey, V. Kinetics and mechanism of action of glucose oxidase. *J. Biol. Chem.* **1964**, *239*, 3927−3934.
(34) Duhr, S.; Braun, D. Why molecules move along a temperature gradient. *Proc. Natl. Acad. Sci. U. S. A.* **2006**, *103*, 19678−19682.
(35) Howse, J. R.; Jones, R. A.; Ryan, A. J.; Gough, T.; Vafabakhsh, R.; Golestanian, R. Self-motile colloidal particles: from directed propulsion to random walk. *Phys. Rev. Lett.* **2007**, *99*, 048102.
(36) Ke, H.; Ye, S.; Carroll, R. L.; Showalter, K. Motion Analysis of Self-Propelled Pt−Silica Particles in Hydrogen Peroxide Solutions. *J. Phys. Chem. A* **2010**, *114*, 5462−5467.
(37) Gibbs, J. G.; Zhao, Y. P. Autonomously motile catalytic nanomotors by bubble propulsion. *Appl. Phys. Lett.* **2009**, *94*, 163104.
(38) Ma, X.; Jang, S.; Popescu, M. N.; Uspal, W. E.; Miguel-López, A.; Hahn, K.; Kim, D.-P.; Sánchez, S. Reversed Janus Micro/Nanomotors with Internal Chemical Engine. *ACS Nano* **2016**, *10*, 8751−8759.

DOI: 10.1021/acscentsci.6b00254
ACS Cent. Sci. 2016, 2, 843−849